Int. J. Electrochem. Sci., 15 **(2020)** 3694 – 3703, doi: 10.20964/2020.05.75

International Journal of
ELECTROCHEMICAL
SCIENCE
www.electrochemsci.org

Short Communication

Post-annealed Aluminum-Doped Zinc Oxide/Tin-Doped Indium Oxide Bilayer Films for Low Emissivity Glass

Shang-Chou Chang[1,2,*] *and Huang-Tian Chan* [2]

[1] Department of Electrical Engineering, Kun Shan University, Tainan City 71010, Taiwan
[2] Green Energy Technology Research Center, Kun Shan University, Tainan City 71010, Taiwan
[*]E-mail: jchang@mail.ksu.edu.tw

Received: 5 January 2020 / *Accepted:* 4 March 2020 / *Published:* 10 April 2020

This study uses post-annealed aluminum-doped zinc oxide /tin-doped indium oxide bilayer (AZO/ITO) films for low emissivity glass. The AZO/ITO films are deposited on glass substrates using in-line sputtering. The AZO/ITO films are subjected to either vacuum or hydrogen plasma annealing. The microstructure, the visible transmittance, the electrical properties and the emissivity of as-deposited, vacuum-annealed and plasma-annealed AZO/ITO films are measured. Hydrogen plasma annealing changes the surface morphology of AZO/ITO films. The average visible transmittance increases and the electrical resistivity and emissivity decrease for AZO/ITO films after vacuum or plasma annealing. The vertical cross-section and surface morphology for vacuum-annealed AZO/ITO films is similar to that for as-deposited films. The surface roughness of AZO/ITO films increases and polygonal grains form after plasma annealing. The electrical resistivity of the vacuum-annealed and hydrogen plasma-annealed AZO/ITO films is 59% and 63% less than the value for as-deposited films. The average visible transmittance of the vacuum-annealed and hydrogen plasma-annealed AZO/ITO films is 8.64% and 12.71% greater than the value for as-deposited films. The emissivity of vacuum-annealed and hydrogen plasma-annealed samples is 2.3 times and 2.56 times less than that of as-deposited AZO/ITO films. The emissivity and the average visible transmittance for vacuum-annealed and hydrogen plasma-annealed AZO/ITO films is 0.09 and 81.58% respectively, which is within the range for commercial low emissivity materials.

Keywords: AZO/ITO; vacuum annealing; hydrogen plasma annealing; low emissivity glass

1. INTRODUCTION

Low-emissivity glass (low-e glass) has high visible transmittance and is used for thermal insulation in buildings [1]. Emissivity is the reference index for low-e glass. The emissivity of current reported low-e glass products is less than 0.45 [2]. Silver is the most widely used low emissivity material. Silver's high electrical conductivity results in a low emissivity because of the Hagen-Ruben

relationship [3]. However, silver films are easily oxidized and adhere poorly to a glass substrate. A seed layer and the barrier layer are often added onto and below silver films to prevent oxidation and to improve the optical properties of silver films. Single-layer-silver multilayer films have at least five layers on glass and double (or triple) –layer-silver films that have a lower emissivity can have more than nine layers. The multilayer process increases the production cost for low emissivity glass [3-5]. Alternatives to silver-based multilayer films for low-e glass have been proposed to reduce the production cost for multilayer films. Transparent conductive oxide materials such as tin-doped indium oxide (ITO) and aluminum-doped zinc oxide (AZO) have relatively high visible light transmittance and electrical conductivity are commonly used in flat panels and solar cells. High electrical conductivity corresponds to low emissivity [6-10]. The electrical resistivity of ITO is lower than that of AZO, but the Indium in ITO is a toxic and costly element. This study uses ITO and AZO films to produce low-emissivity glass. Annealing either ITO or AZO films decreases the resistivity of the films [11-13]. Hydrogen plasma treatment decreases the resistivity and increases the carrier concentration for AZO [14, 15]. Previous studies show that hydrogen annealing increases the electrical conductivity of AZO because negatively charged oxygen species are eliminated from the surface of AZO [11, 16]. Negatively charged oxygen species at the grain boundaries act as electron trapping centers and form potential energy barriers so the free carrier concentration and hall mobility are decreased. Desorption of these negatively charged oxygen species during annealing increases the free carrier concentration and hall mobility. Vacuum annealing increases the electrical conductivity of AZO films [12] because oxygen vacancies that act as electron donors are produced during vacuum annealing. Using AZO and ITO bilayer (AZO/ITO) films gives high electrical conductivity and high visible transparency, which are requirements for low emissivity glass [17, 18]. AZO/ITO films are prepared using in-line sputtering and are then post-annealed using either vacuum or hydrogen plasma annealing. The emissivity, electrical conductivity and visible optical transmittance for annealed AZO/ITO films is better than that for as-deposited films.

2. EXPERIMENTS

Glass substrates were ultrasonically rinsed with acetone, purified water and isopropanol. The glass was then dried using dry nitrogen. The AZO/ITO films were deposited on glass substrates using in-line sputtering. The schematic structure of the AZO/ITO films is shown in figure 1. The ITO sputtering target for ITO films was In_2O_3:SnO_2 = 90:10 wt.% in composition and measured 150×1500mm^2. The AZO sputtering target that was used to deposit AZO films was ZnO:Al_2O_3 = 98:2 wt.% in composition and measured 760×136mm^2. The ITO and AZO films were 250 nm thick. The substrate was maintained at room temperature during sputtering. Other process parameters for sputtering ITO films are a 40 sccm in Ar(85%)/O_2(15%) gas flow, 1.6×10^{-3} torr working pressure and 9 kW sputtering power. The parameters for depositing AZO films are a 440 sccm pure Ar gas flow, 3×10^{-3} torr in working pressure and 2kW in sputtering power.

After deposition, the AZO/ITO films were post-annealed in either vacuum or a microwave hydrogen plasma. The AZO/ITO films were post-annealed for 1 hour using a vacuum of 10^{-5} Torr and

a temperature of 400°C. The AZO/ITO films were post-annealed for 5 minutes in microwave hydrogen plasma at 600W, using a gas pressure of 25 torr and a 100 sccm hydrogen flow rate.

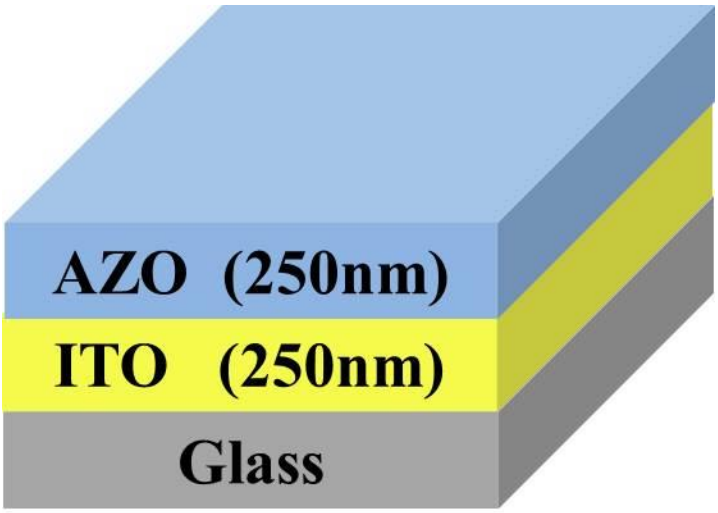

Figure 1. Structure of the fabricated AZO/ITO films.

The cross section of AZO/ITO films was obtained using a Dual-Beam Focused Ion Beam (D-B FIB; FEI Nova NanoLab 200). The crystalline structure of AZO/ITO films was observed using an X-ray diffractometer (XRD; Rigaku D/MAX-2500 V, Rigaku, Tokyo, Japan). The surface morphology of the AZO/ITO films was observed using a Field-Emission Scanning Electron Microscope (FESEM; JEOL JSM-6700 F, JEOL, Tokyo, Japan). The carrier concentration, mobility and electrical resistivity of the AZO/ITO films were measured using a Hall measurement (Ecopia HMS-3000, Ecopia). The visible transmittance of AZO/ITO films was measured using an ultraviolet-visible spectrophotometer (Lambda 750 UV-VIS-NIR spectrometer) for wavelengths of 380~780 nm. The emissivity of the AZO/ITO films was measured using an emissivity meter (TSS-5X, Japan Sensor, Tokyo, Japan).

3. RESULTS AND DISCUSSION

The cross-sectional views of as-deposited and vacuum-annealed AZO/ITO films are similar. Figures 2(a) and 2(b) respectively show cross-sections of as-deposited and hydrogen plasma-annealed AZO/ITO films. The thickness of the AZO/ITO films is 500 nm, as shown in Figure 2(a) and Figure 2(b). The surface of the hydrogen plasma-annealed films is rougher than that of the as-deposited samples, as shown in Figure 2(a) and Figure 2(b).

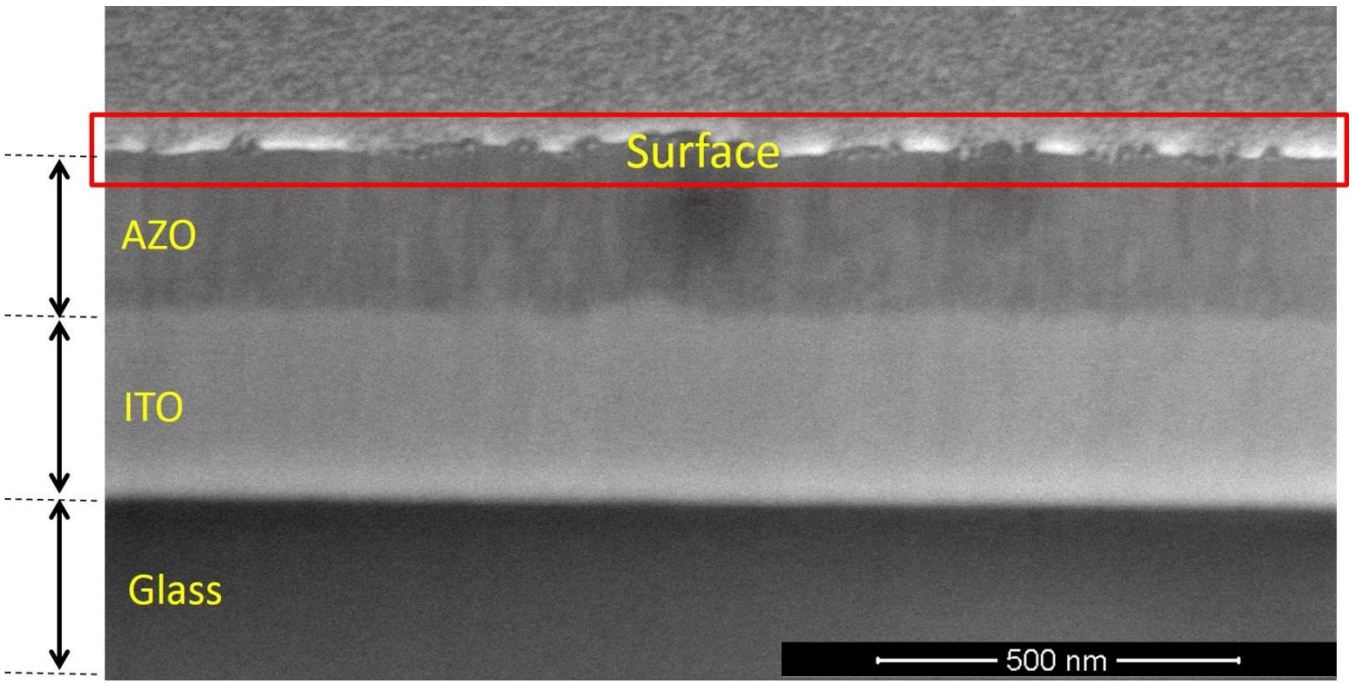

(a)

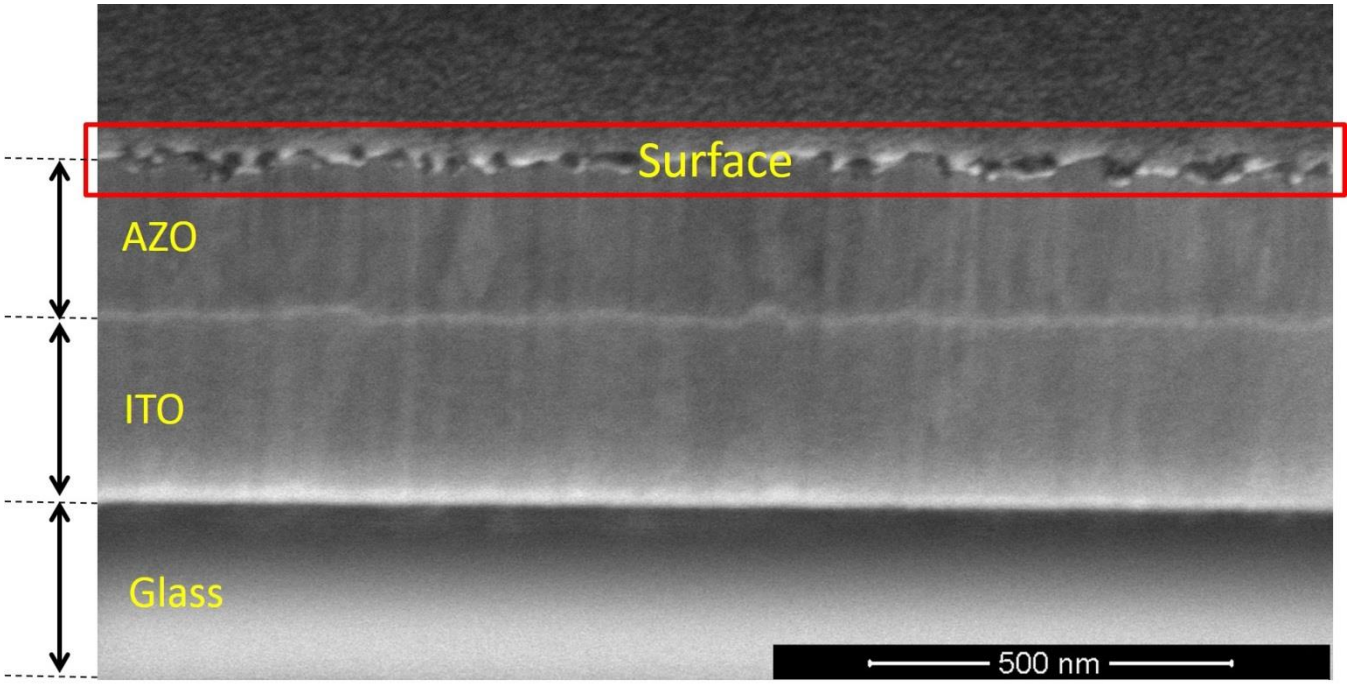

(b)

Figure 2. D-B FIB cross-sectional view of (a) as-deposited and (b) hydrogen plasma-annealed AZO/ITO films.

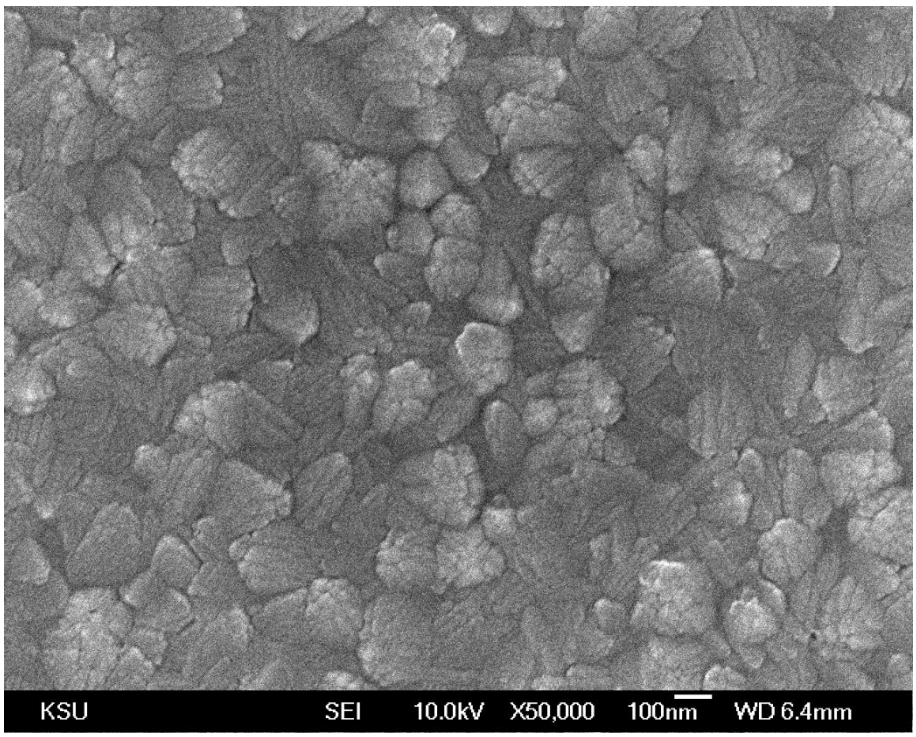

(a)

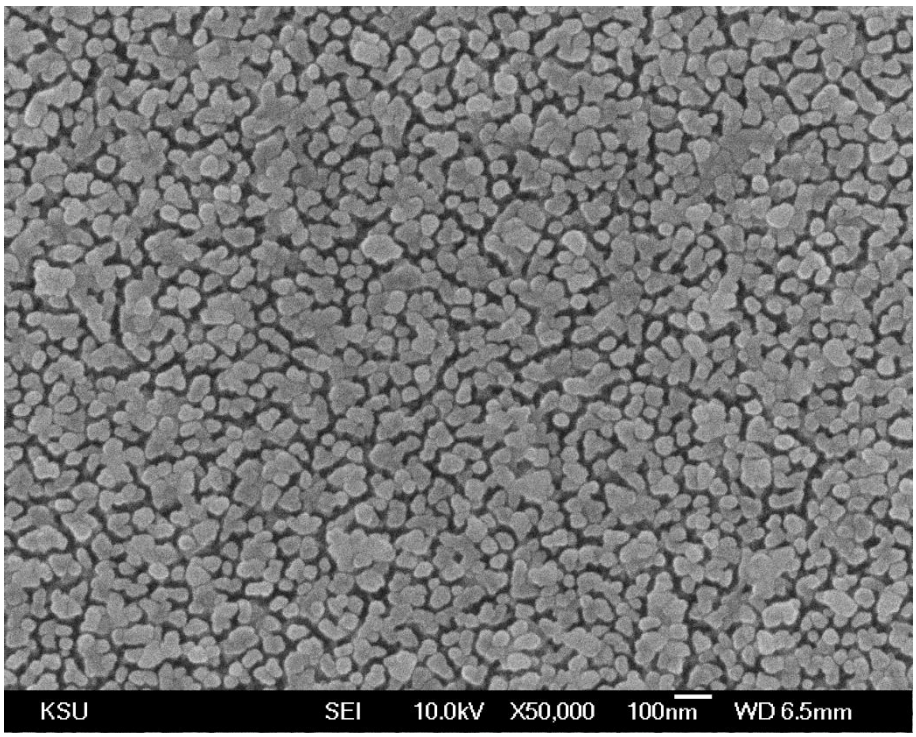

(b)

Figure 3. Micrographs of (a) as-deposited and (b) hydrogen plasma-annealed AZO/ITO films.

The shape and size of the grains in the as-deposited AZO/ITO films are similar to those of vacuum-annealed samples. Figures 3(a) and 3(b) respectively show micrographs of the as-deposited, hydrogen plasma-annealed AZO/ITO films. The AZO/ITO films form polygonal and nano-sized grains after hydrogen plasma-annealing, as shown in Figure 3(b). The surface roughness increases and new

shape grains are formed, as shown in a previous report by the authors that pertains to hydrogen plasma-annealed gallium and aluminum-doped zinc oxide films [19].

Figure 4 shows the XRD spectra for AZO/ITO films that are produced using three sets of conditions. The main (002) peaks for ZnO are clearly observed. Other diffraction peaks include (222), (440), (221) and (662) for the In_2O_3 crystal faces. The two theta data for 28 to 38 degrees in Figure 4 is shown in figure 5. The peak positions for ZnO (002) for as-deposited, vacuum-annealed and plasma-annealed AZO/ITO films are similar to those for as-deposited, as seen in Figure 5.

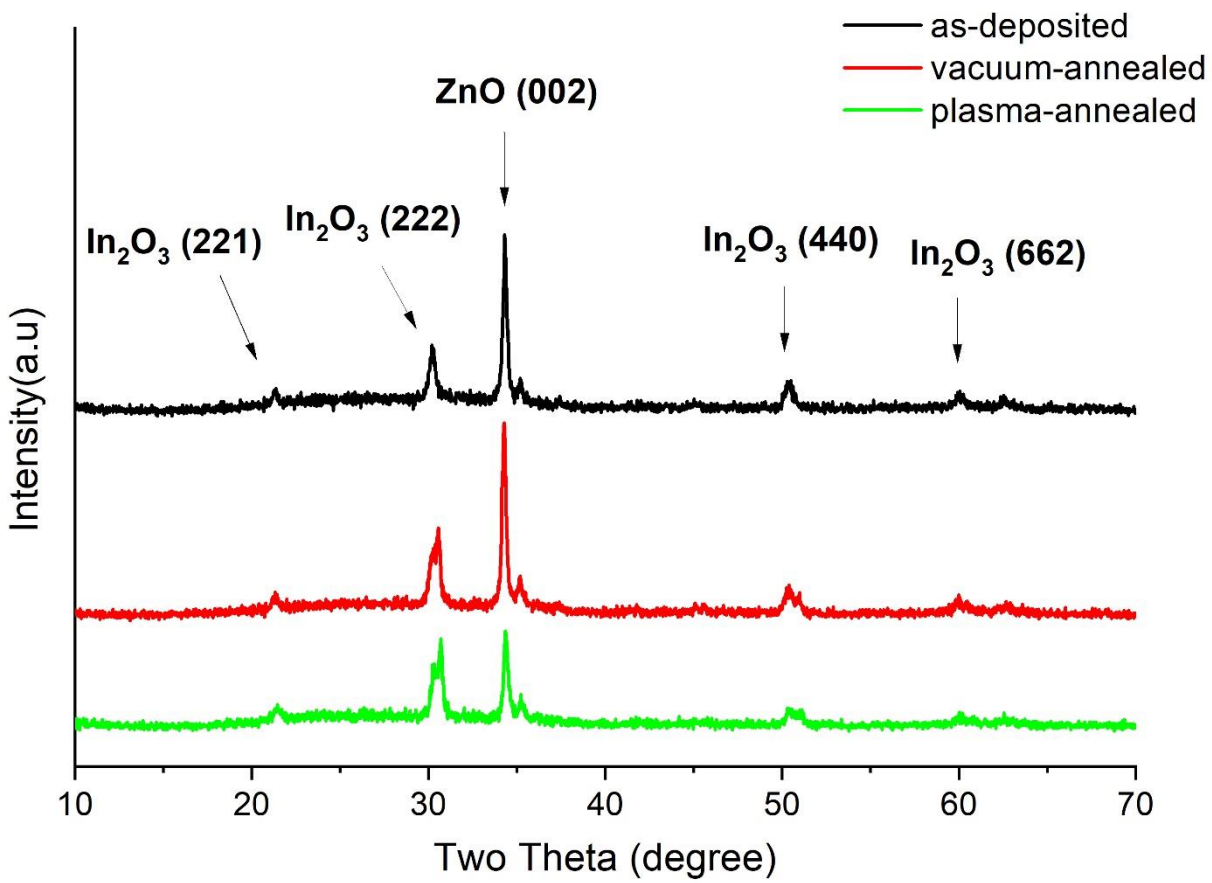

Figure 4. XRD spectra for AZO/ITO that are produced using different methods (as-deposited, vacuum-annealed and hydrogen plasma-annealed).

The peak position for In_2O_3 (222) shifts towards a higher angle for vacuum-annealed and hydrogen plasma-annealed AZO/ITO films. Therefore, the distance between the In_2O_3 (222) planes for post annealed AZO/ITO films decreases. The distance decreases because Sn ions are replaced with the lattice sites of In ions in ITO in post-annealed samples. The radii of the In ions (0.81Å ionic radius and 1.44Å covalent radius) is smaller than the radius of the Sn ion (0.71Å ionic radius of and 1.40Å covalent radius) [20-22]. The distance between In_2O_3 (222) decreases when Sn ions replace In ions in ITO. Therefore, the In_2O_3 (222) peak in Figure 5 shifts to a higher angle.

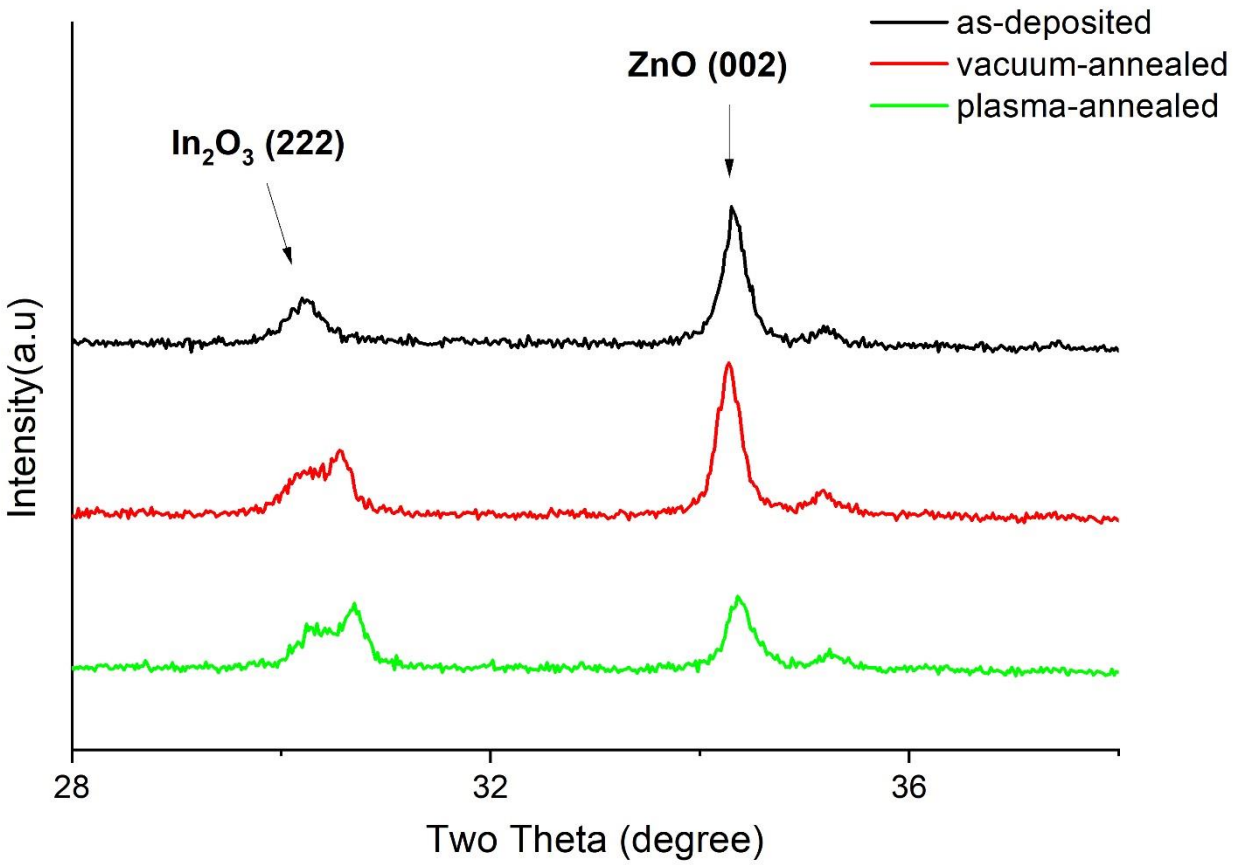

Figure 5. A magnified view of Figure 4 for two theta values of 28-38 degrees.

The electrical properties (carrier density, hall mobility and electrical resistivity) and emissivity of the as-deposited, vacuum-annealed and hydrogen plasma-annealed AZO/ITO films are shown in Table 1. Vacuum annealing and hydrogen plasma annealing both produce an increase in carrier concentration and hall mobility for AZO/ITO films and the electrical resistivity and emissivity are decreased, as shown in Table 1. The results for annealing show that the electrical properties of AZO/ITO films are improved and are in agreement with previous reports on annealed AZO or ITO films [11-16]. Annealing increases carrier concentration because of (i) desorption of negatively charged oxygen species from the grain boundaries, which act as electron trapping centers, and (ii) production of oxygen vacancies in crystals to generate free electrons. Annealing increases the Hall mobility because negatively charged oxygen species are desorbed from the grain boundaries and number of defects acting as electron potential barriers are reduced.

The electrical resistivity of vacuum-annealed, and hydrogen plasma-annealed samples is 59% and 63% less than that of as-deposited samples, as shown in Table 1. The carrier density of AZO/ITO films increases after annealing because Sn ions replace In ions in ITO during annealing so the XRD peaks for In_2O_3 (222) shift to a high angle, as shown in Figure 5. The emissivity of as-deposited, vacuum-annealed and plasma annealed samples is 0.23, 0.10 and 0.09, respectively, as shown in Table 1. The emissivity of vacuum-annealed and hydrogen plasma-annealed samples is 2.3 times and 2.56 times lower than that for as-deposited AZO/ITO films.

Table 1. Electrical properties and emissivity of AZO/ITO films that are produced using different methods.

	Carrier Concentration [$10^{21}cm^{-3}$]	Hall Mobility [cm^2/Vs]	Resistivity [$10^{-4}\Omega$-cm]	Emissivity
as-deposited	2.34	2.71	9.86	0.23
vacuum-annealed	4.12	3.75	4.04	0.10
plasma-annealed	4.91	3.47	3.67	0.09

The emissivity of the materials is related to electrical resistivity found from the Hagen–Rubens relationship [9, 10], which states that emissivity decreases with the electrical resistivity of the materials. The results in Table 1 also agree with the Hagen–Rubens relationship. The electrical resistivity and emissivity of the AZO/ITO films decrease after vacuum or plasma annealing.

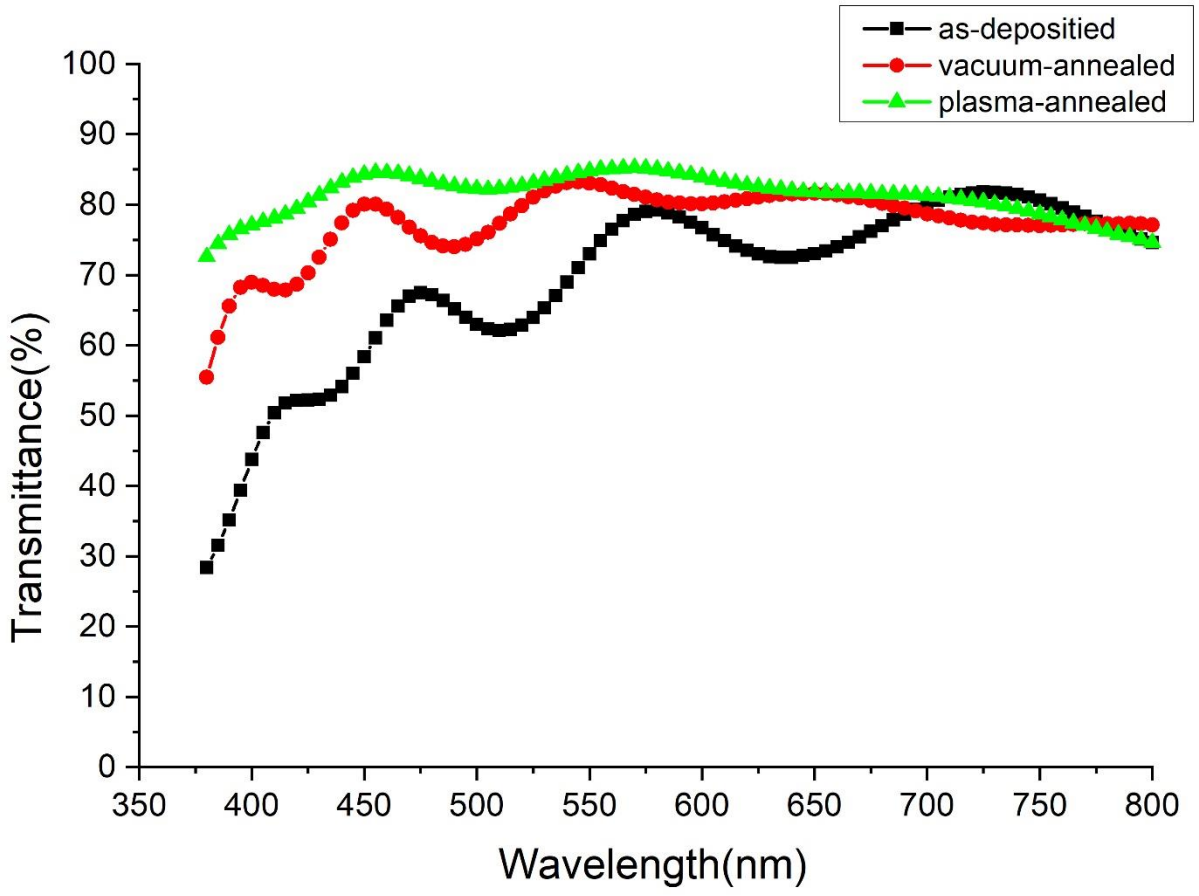

Figure 6. Optical transmittance spectra for AZO/ITO films that are produced using different methods.

Figure 6 shows the visible transmission spectrum for as-deposited, vacuum-annealed and hydrogen plasma-annealed AZO/ITO films. The average respective visible transmittance of as-deposited, vacuum-annealed and hydrogen-plasma annealed samples is 68.87%, 77.51% and 81.58%.

Annealing reduces the number of defects in AZO/ITO films so the visible transmittance of the vacuum- or plasma-annealed samples is greater than that of as-deposited films. The surface roughness is greater for plasma-annealed AZO/ITO films, as shown in Figure 2, so light is not reflected to the same degree.

The transmission spectrum in Figure 6 shows that the transmission curve for hydrogen plasma-annealed AZO/ITO films fluctuates less than those for as-deposited or vacuum-annealed AZO/ITO films. The transmission curve fluctuates because there is interference between the visible wavelength and the thickness of the AZO/ITO films [17]. Previous studies of AZO thin films show that the fluctuations in amplitude decrease because interference is increased due to an increase in the surface roughness of hydrogen plasma-annealed films [19].

The average visible transmittance and emissivity are the reference indices for low-e glass. The hydrogen plasma-annealed AZO/ITO films have an average visible transmittance of 81.58% and an emissivity of 0.09 so they are more suited to construction applications than other recently reported alternatives [2].

4. CONCLUSIONS

AZO/ITO films are produced using in-line sputtering and undergo either vacuum or hydrogen plasma annealing. The surface roughness of hydrogen plasma-annealed AZO/ITO films is increased and polygonal grains form. Vacuum and hydrogen plasma annealing improve the electrical and optical properties of AZO/ITO films. The electrical resistivity of hydrogen plasma-annealed samples is 63% less than that of as-deposited samples. The emissivity of hydrogen plasm- annealed AZO/ITO films is 0.09, which is 2.56 times lower than that the value for as-deposited AZO/ITO films. The electrical resistivity and emissivity of AZO/ITO films decrease after vacuum or hydrogen plasma annealing. This behavior complies with the Hagen–Rubens relationship. The average visible transmittance of hydrogen plasma-annealed samples is 81.58% which is 12.71% greater than the value for as-deposited samples. Hydrogen plasma-annealed AZO/ITO films have a high visible transmittance and low emissivity so they represent a viable commercial alternative for low emissivity glass.

ACKNOWLEDGEMENTS
The authors thank the Ministry of Science and Technology, Taiwan, for its financial support under Contract No's. MOST 105-2221-E-168-101 and MOST 106-2221-E-168-021. This work is partially supported by the Green Energy Technology Research Center.

References

1. D. -C. Tsai, Z.-C. Chang, B.-H. Kuo, E.-C. Chen, Y.-L. Huang, T.-J. Hsieh, F.-S. Shieu, *Ceramics International*, 46(2020)7991.
2. B. P. Jelle, S. E. Kalnæs, T. Gao, *Energy and Buildings*, 96(2015)329.
3. N. Nikitenkov, Modern Technologies for Creating the Thin-film Systems and Coatings, InTechOpen, (2017) London, United Kingdom.

4. R. J. Martõn-Palma, L. Vazquez, J. M. Martõnez-Duart, R. Malats, *Solar Energy Materials and Solar Cells*, 53(1998)55.
5. A. A. Solovyev, S. V. Rabotkin, and N. F. Kovsharov, *Materials Science in Semiconductor Processing*, 38(2015)373.
6. X. Shen, M. Yang, C. Zhang, Z. Qiao, H. Wang, C. Tang, *Superlattices and Microstructures*, 123(2018)251.
7. F. Giovannetti, S. Föste, N. Ehrmann, G. Rockendorf, *Solar Energy*, 104(2014)52.
8. P. Dhamodharan, C. Manoharan, M. Bououdina, R. Venkadachalapathy, S. Ramalingam, *Solar Energy*, 141(2017)127.
9. E. Hagen, H. Rubens, *Annalen der Physik*, 11(1903)873.
10. R. E. Hummel, Electronic Properties of Materials, Springer, (2011) New York, United States.
11. B. Y. Oh, M. C. Jeong, D. S. Kim, W. Lee, J. M. Myoung, *Journal of Crystal Growth*, 281(2005)475.
12. G. Fang, D. Li, B. L. Yao, *Vacuum*, 68(2003)363.
13. M. Asemi, M. Ahmadi, M. Ghanaatshoar, *Ceramics International*, 44(2018)12862.
14. M. F. Al-Kuhaili, *Journal of Materials Science: Materials in Electronics*, 31(2020)2729.
15. M. Morales-Masis, L. Ding, F. Dauzou, Q. Jeangros, A. Hessler-Wyser, S. Nicolay, C. Ballif, *APL Materials*, 2(2014)096113.
16. Y. Takahashi, M. Kanamori, A. Kondoh, H. Minoura, Y. Ohya, *Japanese Journal of Applied Physics*, 33(1994)6611.
17. G. Fang, D. Li, B. L. Yao, *Journal of Physics D Applied Physics*, 35(2002)3096.
18. J.-H. Yun, J. Kim, *Materials Letters*, 70(2012)4.
19. S. C. Chang, *Nanoscale Research Letters*, 9(2014)562.
20. C. Kittel, Introduction to Solid State Physics, John Wiley & Sons, Inc., (2004) Hoboken, NJ, United States.
21. B. R. Koo, J. W. Bae, H. J. Ahn, *Ceramics International*, 43(2017)6124.
22. S. H. Chan, M. C. Li, H. S. Wei, S. H. Chen, C. C. Kuo, *Journal of Nanomaterials*, 2015(2015)179804.